ACS OMEGA

Open Access

http://pubs.acs.org/journal/acsodf

Article

Optimization of Shut-In Time for Hydraulic Fracturing-Assisted Oil Displacement in Offshore Low-Permeability Reservoirs

Baojiang Duan, Qi Li, Zhenhua Cai, Kang Jiang, Fengjiao Wang, Yikun Liu, Mingxuan Chu,* Mengyao Ren, Zhiming Yan, and Qiang Xie

Cite This: *ACS Omega* 2025, 10, 12530−12542

Read Online

ACCESS | Metrics & More | Article Recommendations

ABSTRACT: To optimize the shut-in time for hydraulic fracturing assisted oil displacement in offshore low-permeability reservoirs, a coupled mathematical model encompassing injection, shut-in well, and production is established. The accuracy of the model is validated using production data. The law of pressure diffusion and oil−water two-phase flow during the shut-in well process is clarified, and the mechanism of hydraulic fracturing assisted oil displacement to enhance oil recovery is summarized. The sensitivity analysis is conducted, and then the main controlling factors affecting the optimal shut-in time for hydraulic fracturing assisted oil displacement are identified. The research results indicate that the primary function of the shut-in well is to enhance the effect of formation energy supplementation after injection, thereby further increasing the swept volume, controlling greater geological reserves, and ultimately enhancing oil recovery. During the initial stage of shut-in well, a larger portion of geological reserves are controlled mainly by fluid pressure diffusion, while in the later stage, oil−water exchange is mainly achieved by imbibition effect. The main controlling factors affecting the shut-in time are cumulative injection volume, formation pressure coefficient before hydraulic fracturing assisted oil displacement, and permeability, which should be given special attention on site. The research results provide a theoretical basis for the design of shut-in time for hydraulic fracturing assisted oil displacement operations in offshore low-permeability reservoirs.

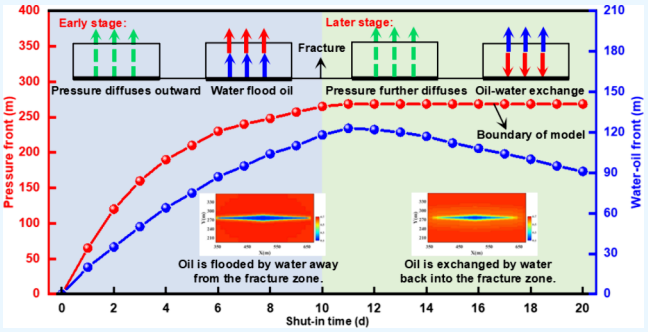

1. INTRODUCTION

In offshore low-permeability reservoirs, due to the large number and complex distribution of faults, small fault block oil reservoirs with independent oil−water systems are formed, which makes it difficult to establish effective displacement relationships. The permeability ranges from 5 to 25 mD, and the porosity is distributed between 10% and 18%. The reservoirs have low porosity and low permeability characteristics and are classified as Type II low-permeability reservoirs. In these reservoirs, depletion development is adopted, which leads to a number of problems. For example, the low level of the formation pressure, the rapid decline of the oil production, the difficulty of stable oil production and the low recovery.[1] The formation pressure coefficient predominantly ranges between 0.50 and 0.90 after the depletion development. Hydraulic fracturing assisted oil displacement (HFAOD) is used to enhance oil recovery of offshore low-permeability reservoirs, building on the experience of the onshore oilfield development. HFAOD is a new enhanced oil recovery technology combining the benefits of fracturing and chemical flooding, which consists of three main stages: injection, shut-in well, and production. Chemical oil displacement agents (surfactant), also known as hydraulic fracturing assisted oil displacement fluid (HFAOD fluid), are pumped into the reservoir through production wells at high pressure and high rate. Low-viscosity HFAOD fluid infiltrates the reservoir during fracturing, effectively supplementing the formation energy.[2−4] The combined effects of fracturing, infiltration to supplement formation energy and HFAOD fluid can significantly increase the oil production of offshore low-permeability reservoirs. The HFAOD technology includes both forward HFAOD and reverse HFAOD. Forward HFAOD refers to injection into an injection well, whereas reverse HFAOD refers to injection into a production well. HFAOD and fracturing followed by huff-and-puff are two distinct reservoir modification techniques, with the following key differences: (1) The low-viscosity HFAOD fluid is used by HFAOD to create fractures and promote infiltration. The combined effects of fracturing and infiltration to supple-

Received: January 8, 2025
Revised: March 1, 2025
Accepted: March 6, 2025
Published: March 20, 2025

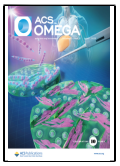

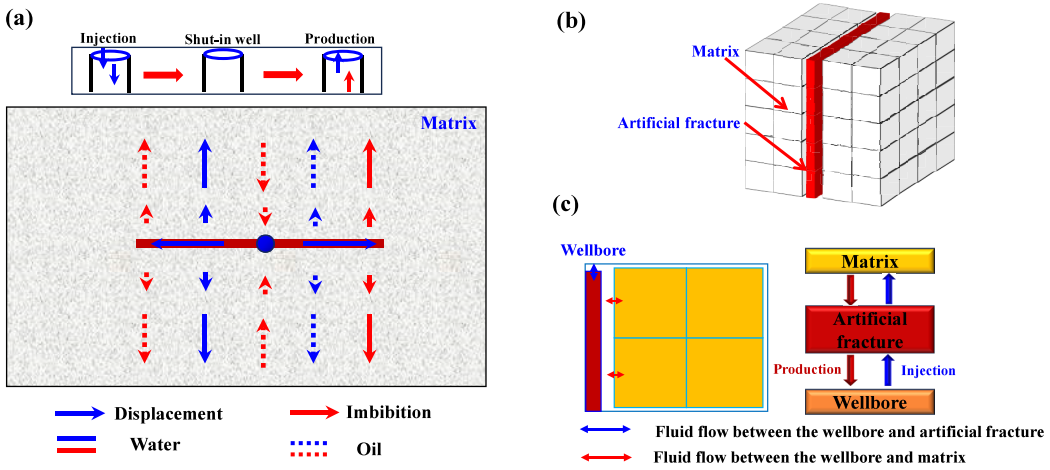

Figure 1. Physical model of FHOAD: Coupled flow in matrix and artificial fracture (a), artificial fracture and matrix (b), and the sequence of fluid flow in wellbore, artificial fracture, and matrix (c).

ment formation energy can control more geological reserves. In contrast, the high-viscosity guanidine gel is used by hydraulic fracture to create fractures, with the aim of minimizing infiltration. The more geological reserves can only be controlled by a fracture. (2) HFAOD is a single process, whereas fracturing followed by huff-and-puff involves two processes: fracturing and huff-and-puff. This study is mainly focused on the optimization of shut-in time for reverse HFAOD.

The BX well in the Weizhou Oilfield, located in the western South China Sea, is the first large-scale HFAOD experimental well that has achieved good development results. Before HFAOD, the production efficiency was poor, with daily oil production of only 24 m^3/d. After HFAOD, the daily oil production stabilized at 120 m^3/d, which is five times the previous oil production rate.[5−7] The cumulative increase in oil production exceeded that of conventional fracturing wells. Moreover, the shut-in time of HFAOD technology is crucial. Prolonged shut-in time results in further diffusion of fluid pressure. During the production process, the energy that diffuses to distant areas is not utilized promptly and effectively, reducing the effect of the cumulative increase in oil production. Conversely, if the shut-in time is too short or no shut-in well is performed, the fluid pressure fails to diffuse, resulting in a limited swept volume. The injected HFAOD fluid will return along the original path and will not be able to achieve an increase in oil production. Therefore, there exists an optimal shut-in time of HFAOD that ensures the supplementary energy can control the maximum geological reserves while minimizing energy wastage. How to determine the optimal shut-in time for offshore low-permeability reservoirs has become an urgent problem that needs to be solved.

Wang et al.[8−12] developed a multiphase flow model encompassing fracturing, shut-in well, and production for shale reservoirs. They found that cumulative increase in oil production initially increased rapidly and then tended toward a stable value as the shut-in time increased, and that the shut-in time corresponding to the inflection point of the change was the optimal shut-in time. Bui et al.[13−16] suggested that filtration of the fracturing fluid into the reservoir could increase the elastic energy and that the shut-in well could improve cumulative oil production. In addition, if the reservoir is oil-wetting, the addition of surfactants to the fracturing fluid could further change the wetting during the shut-in well process, thereby increasing cumulative oil production. Based on the principle of saturation rebalancing, Xu et al.[17−21] proposed an optimization method for the shut-in time of horizontal wells after volume fracturing, with the aim of shortening the oil breakthrough time. They found that if the shut-in time was too short, the oil−water exchange was not enough, resulting in a longer oil breakthrough time. Conversely, if the shut-in time was too long, although the oil−water exchange might have been enough, the energy dissipation near the bottom of the well became severe, resulting in a decrease in cumulative oil production. Wang et al.[22−25] developed a two-dimensional numerical model of multiphase flow and found that prolonging the shut-in time could increase the cumulative oil production. Furthermore, research on the optimization of shut-in time after fracturing for unconventional reservoirs, such as tight oil and shale oil, has been widely reported. Wang et al.[26,27] suggested that the shut-in process after fracturing in shale oil reservoirs was influenced by reservoir properties, wettability, crude oil viscosity, and injection parameters, and the optimal shut-in time was determined to be 64 days. Xu et al.[28,29] found that the imbibition effect was jointly controlled by pressure difference, osmotic pressure and capillary force during the shut-in process after fracturing in the shale oil reservoir. Compared to the pressure difference, the combined effect of osmotic pressure and capillary pressure, the imbibition equilibrium time was reduced from 150 days to 45 days, which was regarded as the lower limit for the shut-in time. Chen et al.[30,31] suggested that the pressure was rapidly diffused within the matrix during the shut-in process after fracturing in shale oil reservoirs. After shut-in well for 65 days, the same pressure was achieved in the entire reservoir, and the imbibition equilibrium was reached. Gu et al.[32,33] found that the pressure decreased with increasing diffusion distance during the shut-in process after fracturing in tight oil reservoirs. The study also demonstrated that the shut-in could effectively enhance oil production. The optimal shut-in time was determined to be 90 days. Zhang et al.[34] suggested that although the shut-in after fracturing in the shale reservoirs might have reduced the initial production, it effectively slowed down the decline in production and maintained long-term production. The optimal shut-in time was determined to be 60 days. Additionally, the shut-in time on site is mostly distributed between 10 to 35 days for offshore low-permeability reservoirs after fracturing, mainly relying on the experience of developers and lacking scientific and reasonable

https://doi.org/10.1021/acsomega.5c00204
ACS Omega 2025, 10, 12530−12542

basis. In summary, the shut-in time is influenced by multiple factors. Moreover, most scholars have primarily focused on the shut-in time after fracturing, with few reports addressing the shut-in time after HFAOD. It is still unknown how different factors affect the optimal shut-in time for offshore low-permeability reservoirs.

In this work, a coupled flow in matrix and artificial fracture mathematical model encompassing injection, shut-in well, and production is established. The accuracy of the model is validated using production data. The law of pressure diffusion and oil−water two-phase flow during the shut-in well process is clarified, and the mechanism of enhanced oil recovery by HFAOD is summarized. The shut-in time is optimized with the objective of maximizing the cumulative increase in oil production. A sensitivity analysis is conducted considering five factors: permeability, formation pressure coefficient before HFAOD, cumulative injection volume, injection rate, and viscosity of the HFAOD fluid. Finally, the main controlling factors affecting the optimal shut-in time of HFAOD are determined. This study establishes a theoretical foundation for optimizing the shut-in time of HFAOD in offshore low-permeability reservoirs. By refining the HFAOD process, it enhances the cumulative increase in oil production and effectively addresses the challenge of determining the optimal shut-in time. Furthermore, it plays a crucial role in promoting the broader application of HFAOD technology in such reservoirs.

2. THEORY AND METHODS

2.1. Mathematical Model. *2.1.1. Physical Model and Assumptions.* The HFAOD technology primarily includes three continuous processes: injection, shut-in well, and production. A physical model of FHOAD coupled flow in matrix and artificial fracture is established, which consists of the wellbore, artificial fracture, and matrix (Figure 1). Injection is a process in which fractures are created by high pressure, and the HFAOD fluid is transported to a distant location in the matrix. Shut-in well is the process by which the fluid pressure and saturation fields are redistributed by imbibition and displacement effects. Production is the process of predicting oil and water production. Therefore, the entire process of FHOAD can be calculated. In the injection process, the fluid primarily flows from the wellbore to the artificial fracture, and then to the matrix. In the production process, fluid flows from the matrix to artificial fracture, and then to the wellbore.

The fracture formed and the HFAOD fluid transported to a distant location of the matrix can effectively supplement the formation energy, thereby expanding the swept volume. HFAOD fluid is a surfactant that effectively reduces oil−water interfacial tension and improves wettability. These changes lead to a decrease in residual oil saturation, thereby enhancing displacement efficiency. In addition, the energy carried by the HFAOD fluid improves connectivity, which increases porosity and permeability, and reduces rock surface roughness, which improves wettability. Ultimately, these result in improved flowability of the oil phase. Based on the above mechanism of enhanced oil recovery and the physical model of HFAOD coupled flow in matrix and artificial structure, the mathematical model is established.

In the mathematical model, the coupled process of the fracture creation by HFAOD fluid and the infiltration of HFAOD fluid in the matrix is equivalently represented as two independent processes: fracture propagation and infiltration. The process is characterized using the presetting fractures method (Figure 1). First, a fracture with a specific geometry and conductivity is artificially created. Then, the HFAOD fluid is injected through production wells into the reservoir containing both a fracture and matrix to characterize the infiltration. During this process, the fracture half-length remains constant without further propagation. It is important to note that HFAOD technology forms vertical fractures in offshore low-permeability reservoirs. Model derivation is based on the following assumptions: (1) The fluid flows isothermally. (2) The system contains three components: oil, water, and HFAOD fluid. Oil and water are immiscible, HFAOD fluid only exist in the aqueous phase, and the adsorption and diffusion of the HFAOD fluid are considered. (3) The capillary force and gravity are considered. (4) the natural fractures are not considered.

2.1.2. Continuity Equation. Based on the conservation of mass and Darcy's law, the capillary force, gravity and crossflow between the matrix and the artificial fracture are considered. The continuity equations of the water, oil phases in the matrix and the artificial fracture are established.[35−37]

$$\nabla\left[\frac{K_{\mathrm{m}}K_{\mathrm{rm(o,w)}}}{B_{\mathrm{(o,w)}}\mu_{\mathrm{(o,w)}}}(\nabla p_{\mathrm{m(o,w)}} - \rho_{\mathrm{(o,w)}}g\nabla D)\right] - \frac{\alpha_{\mathrm{(o,w)}}K_{\mathrm{m}}}{\mu_{\mathrm{(o,w)}}}\nabla(p_{\mathrm{m(o,w)}} - p_{\mathrm{f(o,w)}}) = \frac{\partial}{\partial t}\left[\frac{S_{\mathrm{m(o,w)}}\phi_{\mathrm{m}}}{B_{\mathrm{(o,w)}}}\right] \tag{1}$$

$$\nabla\left[\frac{K_{\mathrm{f}}K_{\mathrm{rf(o,w)}}}{B_{\mathrm{(o,w)}}\mu_{\mathrm{(o,w)}}}(\nabla p_{\mathrm{f(o,w)}} - \rho_{\mathrm{(o,w)}}g\nabla D)\right] + \frac{\alpha_{\mathrm{(o,w)}}K_{m}}{\mu_{\mathrm{(o,w)}}}\nabla(p_{\mathrm{m(o,w)}} - p_{\mathrm{f(o,w)}}) = \frac{\partial}{\partial t}\left[\frac{S_{\mathrm{f(o,w)}}\phi_{\mathrm{f}}}{B_{\mathrm{(o,w)}}}\right] \tag{2}$$

where K is the absolute permeability, mD; K_r is the relative permeability, dimensionless; D is the depth of reservoir, m; S is the saturation, dimensionless; ϕ is the porosity, dimensionless; B is the volume factor, dimensionless; μ is the viscosity, mPa·s; p is the pressure, MPa; α is the shape factor, dimensionless; The subscripts m and f represent the matrix and the artificial fracture, respectively; The subscripts o and w represent the oil and water phases, respectively.

In eqs 1-2, the left side represents the flow and crossflow terms of the oil and water phases, while the right side is the accumulation term for each phase.

The physical properties of the artificial fracture greater than the matrix, such as porosity and permeability. The effects of adsorption and diffusion are considered in the flow of the HFAOD fluid in the matrix, and the effect of diffusion is only considered in the flow of the HFAOD fluid in the matrix. The crossflow between the matrix and the artificial fracture is considered. The continuity equations of the HFAOD fluid in the matrix and the artificial fracture are

$$\nabla\left[\frac{K_{\mathrm{m}}K_{\mathrm{rmw}}C_{\mathrm{s}}}{B_{\mathrm{w}}\mu_{\mathrm{w}}}(\nabla p_{\mathrm{mw}} - \rho_{\mathrm{w}}g\nabla D) + \phi_{\mathrm{m}}S_{\mathrm{mw}}m_{\mathrm{s}}^{\mathrm{D}}\right] - \frac{\partial}{\partial t}[(1-\phi_{\mathrm{m}})\rho_{\mathrm{R}}C_{\mathrm{s}}^{\mathrm{a}}] - \left[\frac{\alpha_{\mathrm{w}}K_{\mathrm{m}}C_{\mathrm{s}}}{\mu_{\mathrm{w}}}\nabla(p_{\mathrm{mw}} - p_{\mathrm{fw}}) + \nabla(\phi_{\mathrm{m}}S_{\mathrm{mw}}m_{\mathrm{s}}^{\mathrm{D}})\right] = \frac{\partial}{\partial t}\left[\frac{S_{\mathrm{mw}}\phi_{\mathrm{m}}C_{\mathrm{s}}}{B_{\mathrm{w}}}\right] \tag{3}$$

$$\nabla\left[\frac{K_{\mathrm{f}}K_{\mathrm{rfw}}C_{\mathrm{s}}}{B_{\mathrm{w}}\mu_{\mathrm{w}}}(\nabla p_{\mathrm{fw}} - \rho_{\mathrm{w}}g\nabla D) + \phi_{\mathrm{f}}S_{\mathrm{fw}}m_{\mathrm{s}}^{\mathrm{D}}\right] + \left[\frac{\alpha_{\mathrm{w}}K_{\mathrm{m}}C_{\mathrm{s}}}{\mu_{\mathrm{w}}}\nabla(p_{\mathrm{mw}} - p_{\mathrm{fw}}) + \nabla(\phi_{\mathrm{m}}S_{\mathrm{mw}}m_{\mathrm{s}}^{\mathrm{D}})\right] = \frac{\partial}{\partial t}\left[\frac{S_{\mathrm{fw}}\phi_{\mathrm{f}}C_{\mathrm{s}}}{B_{\mathrm{w}}}\right] \tag{4}$$

https://doi.org/10.1021/acsomega.5c00204
ACS Omega 2025, 10, 12530−12542

where C_s is the mass concentration of HFAOD fluid, kg/m^3; C^D_s is the diffusion concentration of HFAOD fluid, kg/kg; C^a_s is the adsorption concentration of HFAOD fluid, kg/kg; ρ_R is the rock density, kg/m^3; m_s^D is the diffusion flux of HFAOD fluid, kg/(m^2·s); The subscript s represents the HFAOD fluid.

In eqs 3, the left side represents the flow and diffusion terms, adsorption term, and crossflow term of the HFAOD fluid in the matrix, while the right side is the accumulation term. In eq 4, the left side includes the flow and diffusion terms in the artificial fracture and the crossflow term, while the right side being the accumulation term of the HFAOD fluid.

2.1.3. Auxiliary Equation. To characterize the improvement of porosity and permeability by the HFAOD technology, the compressibility of both the matrix and artificial fractures is considered.

$$\phi_{(m,f)} = \phi_{0(m,f)} e^{C_{(m,f)}(p-p_0)} \tag{5}$$

$$K_{(m,f)} = K_{0(m,f)} e^{E_{(m,f)}(p-p_0)} \tag{6}$$

where ϕ_0 is the initial porosity, dimensionless; K_0 is the initial permeability, mD; C is the compression coefficient, MPa^{-1}; E is the stress sensitivity coefficient, MPa^{-1}; p_0 is the initial fluid pressure, MPa.

The saturation equation is

$$S_{(m,f)o} + S_{(m,f)w} = 1 \tag{7}$$

In the reservoir, the water phase is wetting and the oil phase is nonwetting. The dynamic force capillary was used to characterize the effect of imbibition on the development effect of the HFAOD technology. The capillary force equation is

$$p_c(S_{mw}) = p_{mo} - p_{mw} \tag{8}$$

where p_c is the capillary force, MPa.

In the actual reservoir, the wettability and permeability are influenced by the high pressure and high speed of HFAOD. At the same time, the wettability and interfacial tension are influenced by the physicochemical properties of the HFAOD fluid. Furthermore, the pressure field of HFAOD and concentration field of the HFAOD fluid in the reservoir are heterogeneous, which results in rapid and real-time changes in the microstructure, physical properties, interfacial tension, and wettability at different locations within the reservoir. The rapid and real-time changes in capillary force are induced by these variations, which consequently exerts a substantial influence on the imbibition effect. The imbibition effect is recognized as a critical factor controlling the flow and distribution of HFAOD fluid in low-permeability reservoirs. Therefore, the capillary force needs to be extended from a static to a dynamic description in order to accurately represent the imbibition effect during HFAOD. If the reservoir is divided into N grids, the pressure and the concentration of HFAOD fluid in each grid will change over time and can be calculated. By combining parameters such as the saturation, adsorption, interfacial tension, wettability, and permeability for each grid at a given time can be determined. According to eq 9, the capillary force in the grid at that moment can be further calculated.

$$P_{cres}(S_{mw}) = P_{clab}(S_{mw}) \frac{\sigma_{res}\cos\theta_{res}}{\sigma_{lab}\cos\theta_{lab}} \sqrt{\frac{K_{lab}}{K_{res}}} \tag{9}$$

where σ is the interfacial tension, MPa; θ is the wetting angle,°. The subscripts lab and res represent the experimental condition and actual reservoir condition, respectively.

The HFAOD fluid influences the capillary number primarily by altering the interfacial tension, which subsequently affects the relative permeability. Referring to the calculation method used in conventional numerical simulation software, the relative permeability curves from laboratory experiments are applied to different locations in the reservoir based on linear interpolation of the capillary number during the development of the HFAOD technology. The interpolation factor m is introduced.

$$m = \frac{\lg(N_c) - \lg(N_c^{min})}{\lg(N_c^{max}) - \lg(N_c^{min})} \tag{10}$$

where N_C is capillary number, dimensionless. The superscripts min and max represent the minimum and maximum concentrations of HFAOD fluid, respectively.

At different capillary numbers, the end points of the relative permeability curve are calculated.

$$S_{wi}^{N_c} = mS_{wi}^{max} - (1-m)S_{wi}^{min} \tag{11}$$

$$S_{or}^{N_c} = mS_{or}^{max} - (1-m)S_{or}^{min} \tag{12}$$

where S_{wi} is the irreducible water saturation, dimensionless; S_{or} is the residual oil saturation, dimensionless.

Normalize the saturation

$$\frac{S_w^{min}(N_c) - S_{wi}^{min}}{1 - S_{wi}^{min} - S_{or}^{min}} = \frac{S_{w1}^* - S_{wi}^{N_c}}{1 - S_{wi}^{N_c} - S_{or}^{N_c}} \tag{13}$$

$$\frac{S_w^{max}(N_c) - S_{wi}^{max}}{1 - S_{wi}^{max} - S_{or}^{max}} = \frac{S_{w2}^* - S_{wi}^{N_c}}{1 - S_{wi}^{N_c} - S_{or}^{N_c}} \tag{14}$$

Finally, the relative permeability by the influence of the concentration of HFAOD fluid is

$$K_{r(w,o)}(S_w, N_c) = mK_{r(w,o)}^{max}(S_{w2}^*, N_c) + (1-m)K_{r(w,o)}^{min}(S_{w1}^*, N_c) \tag{15}$$

The adsorption concentration of the HFAOD fluid is related to the mass concentration.

$$m_s^a = (1-\phi)\rho_R C_s^a \tag{16}$$

where, m^a_s is the adsorption mass of HFAOD fluid, kg/m^3.

Based on Fick's law, the HFAOD fluid diffusion is characterized. The relationship between the diffusion mass and the concentration of the HFAOD fluid is

$$m_s^D = D_s \nabla C_s \tag{17}$$

where D_s is the diffusion coefficient of the HFAOD fluid, m^2/s.

2.1.4. Initial Conditions and Boundary Conditions. The initial conditions are

$$\begin{cases} p_{(o,w)}(x,y,z,t)|_{t=0} = p_{(o,w)}^0 \\ S_{(o,w)}(x,y,z,t)|_{t=0} = S_{(o,w)}^0 \\ C_s(x,y,z,t)|_{t=0} = 0 \end{cases} \tag{18}$$

If the reservoir is closed, the outer boundary conditions are

$$\frac{\partial p_{(o,w)}}{\partial x} = 0, \quad \frac{\partial p_{(o,w)}}{\partial y} = 0, \quad \frac{\partial p_{(o,w)}}{\partial z} = 0 \tag{19}$$

https://doi.org/10.1021/acsomega.5c00204
ACS Omega 2025, 10, 12530−12542

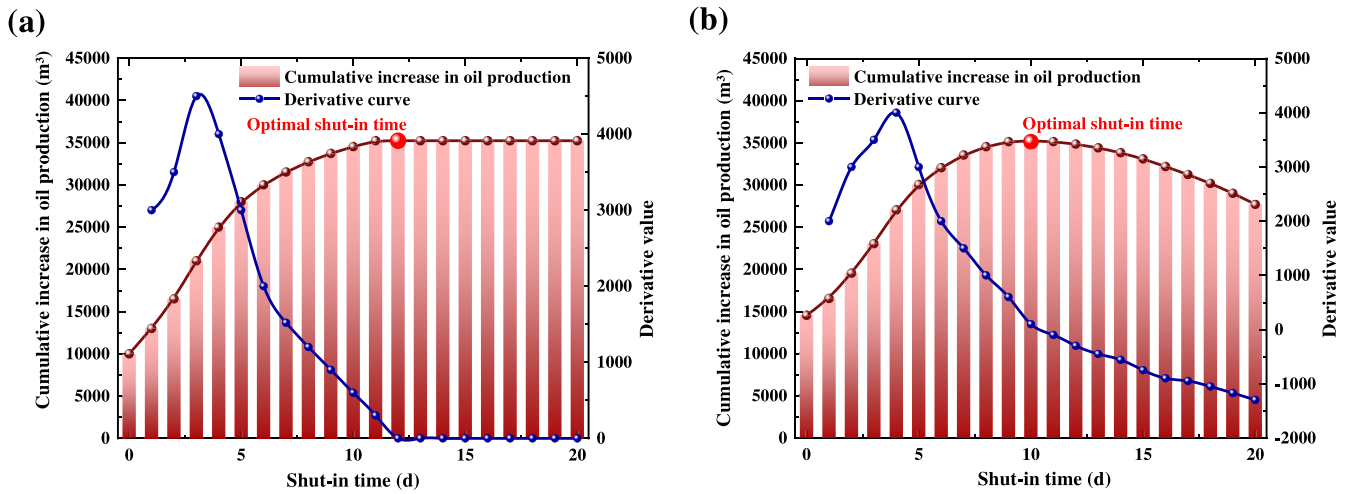

Figure 2. Relationship between cumulative increase in oil production by HFAOD and the shut-in time, where cumulative increase in oil production gradually increases and then slows down (a) or gradually increases and then decreases (b) as the shut-in time increases.

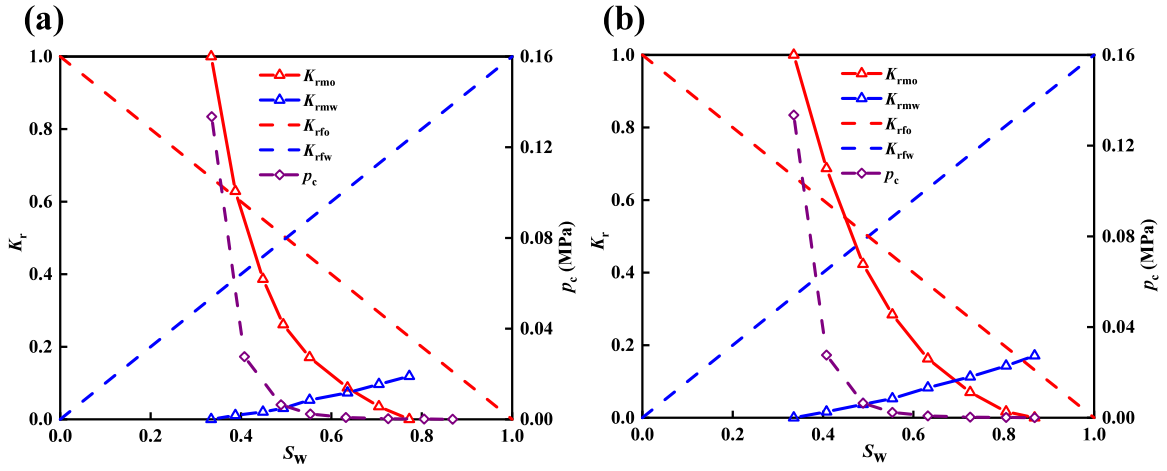

Figure 3. Relative permeability and capillary force curves for the HFAOD fluid concentrations of (a) 0% and (b) 0.35 wt %.

During the production process, the liquid production is fixed, so the inner boundary condition is

$$\frac{\partial p}{\partial r}\Big|_{r=r_w} = \text{constant} \tag{20}$$

In conventional numerical simulations, the imbibition effect in low-permeability reservoirs is typically characterized using the average capillary force measured in the laboratory, with the capillary force assumed to remain static throughout the simulation. Even when a zonal approach is employed, significant errors may be introduced, particularly in the characterization of imbibition phenomena in HFAOD technology for offshore low-permeability reservoirs.[38−40] Rapid and real-time changes in the microstructure, physical parameters, wettability, and oil−water interfacial tension are induced by the high pressure and high speed of HFAOD, thereby affecting the capillary force. In other words, the capillary force is characterized by a time-dependent variation. In this study, the capillary force needs to be extended from a static to a dynamic description to accurately represent the imbibition effect during HFAOD in offshore low-permeability reservoirs. By incorporating the relationships between capillary force, wettability, interfacial tension, and permeability into the numerical simulation, the capillary force at different reservoir locations can be calculated over time, more closely approximating the actual conditions of HFAOD and providing a more reliable basis for optimizing the shut-in time.

2.2. Optimization Method of Shut-In Time. Based on the established mathematical model coupled flow in matrix and artificial fractures, the shut-in time is optimized with the goal of maximizing cumulative increase in oil production. The specific steps as follows:[41,42] (1) Based on known geological and engineering parameters, the cumulative oil production corresponding to different shut-in times is obtained. (2) Based on the results of step (1), the difference between cumulative oil production at different shut-in times and that of depletion development is calculated, and then the relationship between the cumulative increase in oil production by HFAOD and shut-in time is obtained. (3) The relationship between the cumulative increase in oil production by HFAOD and shut-in time show two patterns (Figure 2): (a) The cumulative increase in oil production gradually increases and then slows down with the shut-in time increases (Figure 2a). (b) The cumulative increase in oil production gradually increases and then decreases with the shut-in time increases (Figure 2b). To optimize the shut-in time, the derivative of the relationship between the cumulative increase in oil production by HFAOD and shut-in time is taken. The shut-in time corresponding to the point where the derivative value is zero is the optimal shut-in time.

https://doi.org/10.1021/acsomega.5c00204
ACS Omega 2025, 10, 12530−12542

3. APPLICATION

3.1. Validation. By combining the auxiliary equations, boundary conditions, and basic experimental data such as the relative permeability curves and capillary force curves (Figure 3), the fluid pressure is solved implicitly, and the oil−water saturation and the concentration of the HFAOD fluid are solved explicitly. Then, the sensitivity analysis of the optimal shut-in time for HFAOD in offshore low-permeability reservoirs is conducted.

Wells $L^{\#}$ and $W^{\#}$, located in offshore low-permeability reservoirs, are selected to validate the model. The basic parameters of geology and oil reservoirs are listed in Table 1.

Table 1. Basic Parameters of Geology and Oil Reservoirs

Parameter	Well $L^{\#}$	Well $W^{\#}$
Thickness (m)	29.7	25
Initial formation pressure coefficient	1	1.06
Porosity (%)	26.1	19.25
Permeability (mD)	22.8	20
Formation pressure coefficient before HFAOD	0.88	0.7
Viscosity of HFAOD fluid (mPa·s)	1	1
Injection rate (m^3/min)	5	5
Accumulate injection (m^3)	13,900	13,440
Fracture half-length (m)	150	110
Shut-in time (d)	10	10
Surfactant concentration (%)	0.35	0.35
Matrix compressibility coefficient (MPa^{-1})	1×10^{-4}	1×10^{-4}
Fracture compressibility coefficient (MPa^{-1})	0.1	0.1
Matrix stress sensitivity coefficient (MPa^{-1})	0.01	0.01
Fracture stress sensitivity coefficient (MPa^{-1})	0.1	0.1

Well $L^{\#}$ is located in an independent fault block with a permeability of 22.8 mD, porosity of 26.1%, and an effective thickness of 29.7 m. The formation pressure coefficient before HFAOD at a depth of 2700 m is 0.88. Well $W^{\#}$ is located in a complex fault block with a permeability of 20 mD, porosity of 19.25%, and an effective thickness of 25 m. The formation pressure coefficient before HFAOD at a depth of 2180 m is 0.7. Both wells are isolated well points, lacking an effective injection-production well pattern. Prolonged depletion development has led to a continuous decline in formation pressure, with a recovery factor of less than 10%.

The grid generation process for numerical simulation is shown in Figure 4. A homogeneous grid system is applied along the fracture direction (y-axis), whereas a heterogeneous grid system is applied in the perpendicular direction (x-axis). The grid spacing decreases as the distance to the fracture decreases, and increases as the distance to the fracture increases. Second, during the establishment of artificial fractures, the grid is further refined according to the (7 7 1) method, thereby enabling a more detailed description of the pressure field and saturation field in the vicinity of the fracture. The grid parameters for numerical simulation are listed in Table 2. The fracture half-lengths of Well $L^{\#}$ and Well $W^{\#}$ are 223 and 197 m, respectively.

The oil and water production are calculated fixing liquid production. The calculation results show good agreement with production data obtained on site, as shown in Figure 5. The calculation accuracies for cumulative oil production, cumulative water production and the bottom hole pressure are 99.19%,99.84% and 86.43% for well $L^{\#}$, and 98.46%, 85.1% and 85.88% for well $W^{\#}$. These indicate that the model developed in this work can accurately predict the production dynamics of HFAOD.

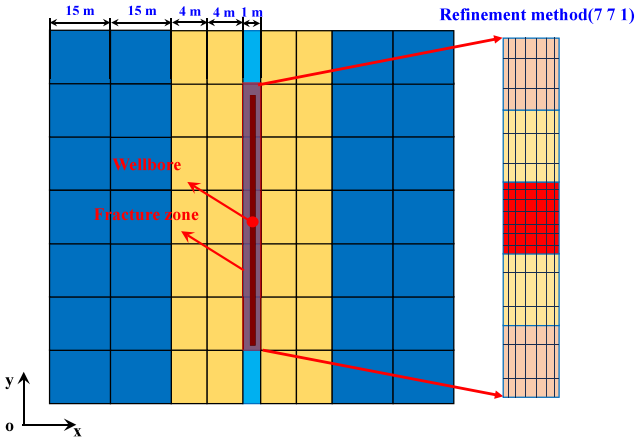

Figure 4. Grid generation process for numerical simulation.

The daily liquid production of well $L^{\#}$ before HFAOD was 3.7 m^3/d, with the daily oil production of 3.5 m^3/d and the formation pressure coefficient of 0.88. Subsequent to the implementation of HFAOD, there was an increase in daily liquid production to 77 m^3/d, daily oil production increased to 33 m^3/d, and the formation pressure coefficient recovered to 1.04. The predicted cumulative increase in oil production is 3.13×10^4 m^3. The daily liquid production of well $W^{\#}$ before HFAOD was 9.4 m^3/d, with the daily oil production of 1.4 m^3/d and the formation pressure coefficient of 0.7. Subsequent to the implementation of HFAOD, there was an increase in daily liquid production to 124 m^3/d, daily oil production increased to 110 m^3/d, and the formation pressure coefficient recovered to 0.89. The predicted cumulative increase in oil production is 3.5×10^4 m^3. A comparison of the production dynamics of the two wells indicates that the implementation of HFAOD technology not only recovered formation pressure, but also significantly improved production capacity and ultimately enhanced oil recovery.

3.2. Law of Pressure Diffusion and Oil−Water Flow. The primary function of the shut-in well is to enhance the effect of formation energy supplementation after injection, thereby further increasing the swept volume, controlling greater geological reserves, and ultimately enhancing oil recovery. Figure 6a, 6b and 6c show the distribution of the fluid pressure at different shut-in times. The fluid pressure front further diffuses in the direction of the vertical fractures. The fluid pressure in the fracture zone gradually decreases, the area swept by the fluid pressure gradually increases, the geological reserves controlled by the HFAOD gradually increase, and the overall fluid pressure field tends to balance. The longer the shut-in time, the more balanced the fluid pressure distribution.

Figure 6d, 6e and 6f show the distribution of the fluid saturation at different shut-in times. The pressure difference controls the displacement effect, while capillary force controls the imbibition effect, and both occur simultaneously during the shut-in well process. In the early stage of shut-in well, displacement plays a dominant role. The fracture is located in a high fluid pressure zone, and the further away from the fracture, the lower the fluid pressure. The HFAOD fluid displaces the crude oil in the reservoir to a distant location. As the fluid pressure gradually balances, the imbibition effect gradually becomes dominant and the crude oil far from the

https://doi.org/10.1021/acsomega.5c00204
ACS Omega 2025, 10, 12530−12542

Table 2. Grid Parameters for Numerical Simulation

Parameter	Well $L^{\#}$	Well $W^{\#}$
Single well control area	1005 × 550 m^2	945 × 537 m^2
Grid size	X: 67 × 15 m, Y: 15 × 15 m, 10 × 4 m, 11 × 2 m, 10 × 4 m, 15 × 15 m	X: 63 × 15 m, Y: 15 × 15 m, 10 × 4 m, 7 × 1 m, 10 × 4 m, 15 × 15 m
Total number of grids before refining the fracture zone	12261	10773
Total number of grids after refining the fracture zone.	13605	12117

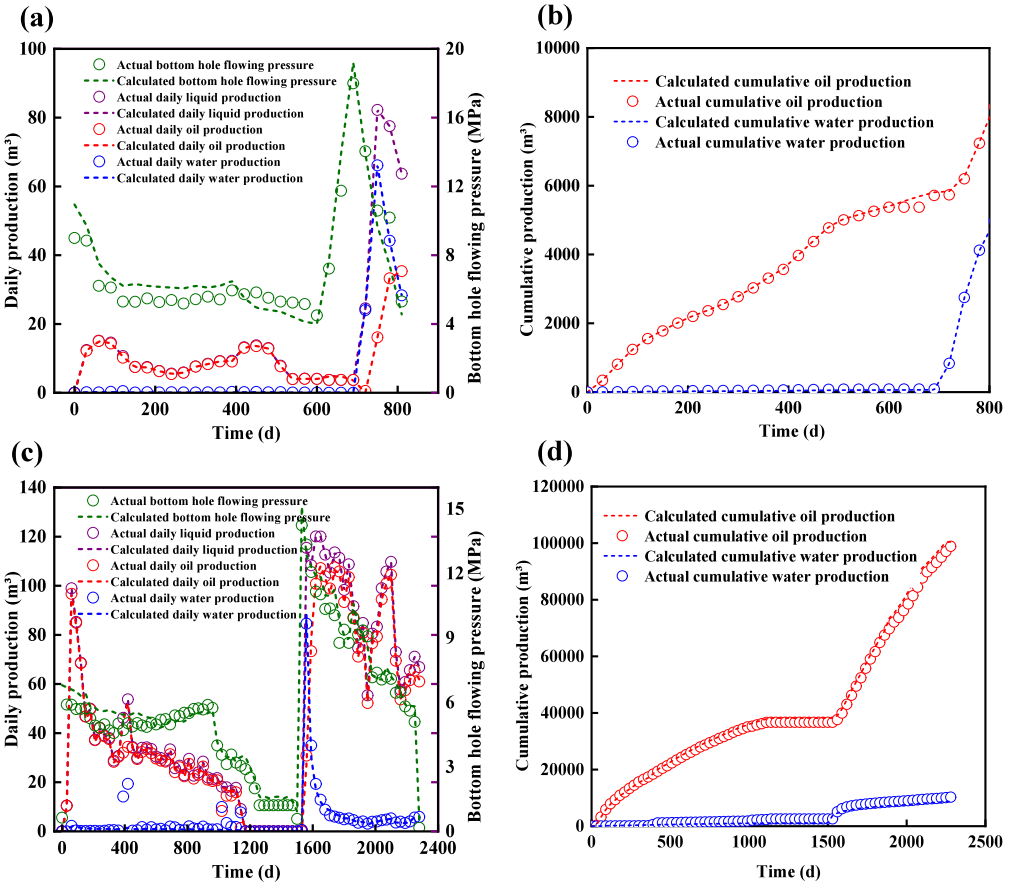

Figure 5. Production dynamic verification of well $L^{\#}$ (a, b) and well $W^{\#}$ (c, d).

fracture zone is exchanged back into the fracture zone. The longer the shut-in time, the more crude oil is exchanged back into the fracture zone.

4. RESULTS AND DISCUSSION

4.1. Sensitivity Analysis. Based on the basic parameters of well $W^{\#}$, the coupled mathematical model is adopted to conduct a sensitivity analysis of the optimal shut-in time considering five factors: permeability, formation pressure coefficient before HFAOD, viscosity of HFAOD fluid, injection rate, and cumulative injection volume. The sensitivity analysis scheme is shown in Table 3.

4.1.1. Permeability. Considering permeabilities of 10, 20, 50, 150, and 400 mD, with corresponding fracture half-lengths of 291, 216, 153, 104, and 83 m. The calculation method for the fracture half-length of HFAOD is primarily based on previously published research results.[43] By coupling the KGD model (Khristianovich-Geertsma-de Klerk model) and the flow tube method, a semianalytical mathematical model for the fracture propagation during HFAOD is developed to account for the effect of infiltration on fracture propagation. Based on this approach, the fracture half-length of HFAOD is calculated in this study.

Figure 7 shows the cumulative increase in oil production and the optimal shut-in time at different permeabilities. It is noteworthy that the colored stripes in Figure 7c indicate errors. The narrower region indicates the 95% confidence interval, reflecting the uncertainty range of the fitted curve parameters. The wider region indicates the prediction band, reflecting the potential range of future observations. The meaning of the colored stripes in Figures 8c, 9c, 10c, and 11c is analogous to that in Figure 7c. The higher the permeability, the faster the fluid pressure diffusion during the shut-in well process, and the shorter the time it takes for the fluid pressure to reach balance. When the permeability is less than 100 mD, the cumulative increase in oil production initially increases with shut-in time and then decreases. Prolonged shut-in time results in further diffusion of fluid pressure. The energy that diffuses to distant areas is not utilized promptly and effectively during the production process. When the permeability is greater than 100

https://doi.org/10.1021/acsomega.5c00204
ACS Omega 2025, 10, 12530−12542

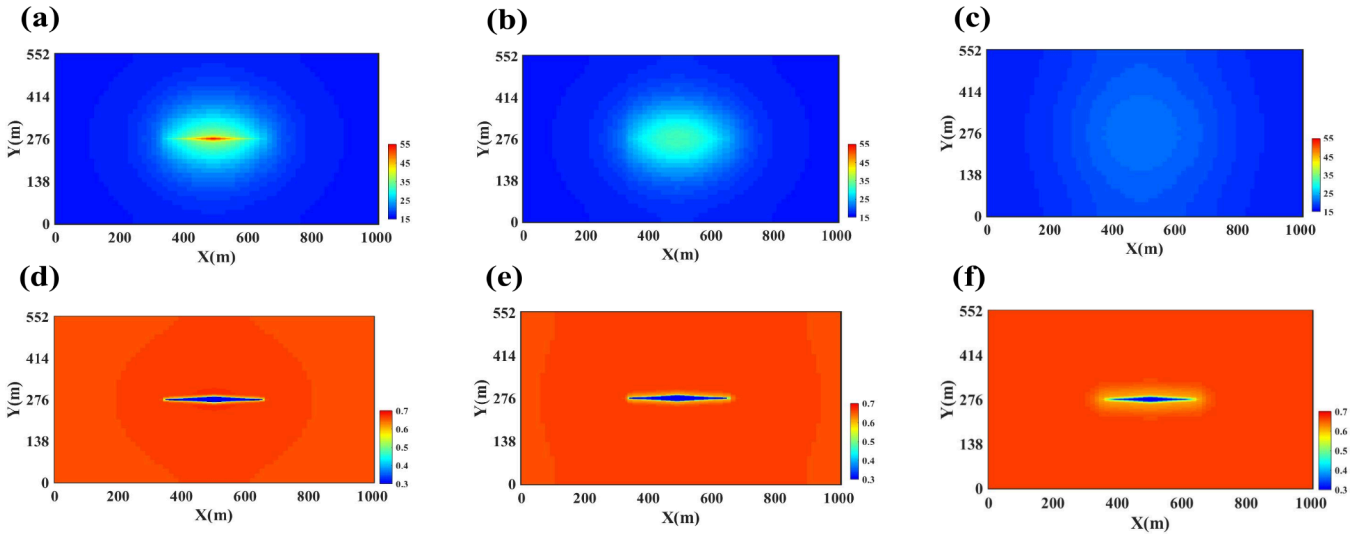

Figure 6. Fluid pressure distribution at shut-in time of 0 days (a), 2 days (b), and 5 days (c) and oil saturation distribution at shut-in time of 0 days (d), 10 days (e), and 20 days (f).

Table 3. Sensitivity Analysis Schemes

Scheme	Permeability (mD)	Formation pressure coefficient before HFAOD	Cumulative injection volume (m^3)	Injection rate (m^3/min)	Viscosity of HFAD fluid (mPa·s)
1	10	0.5	13440	5	1
2	20	0.5	13440	5	1
3	50	0.5	13440	5	1
4	150	0.5	13440	5	1
5	400	0.5	13440	5	1
6	20	0.5	13440	5	1
7	20	0.7	13440	5	1
8	20	1	13440	5	1
9	20	1.3	13440	5	1
10	20	0.5	4800	5	1
11	20	0.5	13440	5	1
12	20	0.5	14400	5	1
13	20	0.5	16000	5	1
14	20	0.5	13440	2	1
15	20	0.5	13440	4	1
16	20	0.5	13440	5	1
17	20	0.5	13440	8	1
18	20	0.5	13440	5	1
19	20	0.5	13440	5	3
20	20	0.5	13440	5	5
21	20	0.5	13440	5	10

mD, the cumulative increase in oil production gradually increases with the shut-in time and then tends to a stable value. High permeability results in rapid fluid pressure diffusion. The energy is quickly transferred to the distant formation during the shut-in well process and quickly returned to the bottom of the well during the production process. The higher the permeability, the more the cumulative increase in oil production by HFAOD. The optimal shut-in time of HFAOD gradually decreases as the permeability increases.

4.1.2. Formation Pressure Coefficient before HFAOD. Considering formation pressure coefficients before HFAOD of 0.5, 0.7, 1, and 1.3, with corresponding fracture half-lengths of 153, 174, 244, and 301 m. Figure 8 shows the cumulative increase in oil production and the optimal shut-in time at different formation pressure coefficients before HFAOD. The higher the formation pressure coefficient before HFAOD, the slower the fluid pressure diffusion during the shut-in well process, and the longer the time it takes for the fluid pressure to reach balance. However, the fracture half-length increases with the increase of the formation pressure coefficient before HFAOD, resulting in a larger area of the imbibition effect. Therefore, more crude oil is exchanged back to the fracture zone for the same shut-in time.

When the formation pressure coefficient before HFAOD is less than 1, the cumulative increase in oil production initially increases with shut-in time and then decreases. Prolonged shut-in time results in further diffusion of fluid pressure. The energy that diffuses to distant areas is not utilized promptly and effectively during production process. The most important way to enhance oil recovery is to enhance the effect of formation energy supplementation to expand the swept volume during shut-in well process. When the formation pressure coefficient before HFAOD is larger than 1, the cumulative increase in oil production initially increases with shut-in time and then ends to a stable value. The energy of the reservoir itself is not deficient, and the most important way to enhance oil recovery is through oil−water exchanged by the imbibition effect during shut-in well process. The higher the formation pressure coefficient before HFAOD, the more the cumulative increase in oil production by HFAOD. The optimal shut-in time of HFAOD gradually increases as the formation pressure coefficient before HFAOD increases.

4.1.3. Cumulative Injection Volume. Considering cumulative injection volumes of 4800, 13440, 14400, and 16000 m^3, with corresponding fracture half-lengths of 146, 153, 153, and 153 m. Figure 9 shows the cumulative increase in oil production and the optimal shut-in time at different cumulative injection volumes. At the same injection rate, a larger cumulative injection volume leads to greater energy accumulation around the fracture zone at the end of injection, causing the fluid pressure front to advance more quickly during the shut-in well process. But the larger the cumulative injection volume, the longer it takes for the fluid pressure to balance. At the same shut-in time, a less cumulative injection volume results in more crude oil being exchanged back into the fracture zone. However, the more the

https://doi.org/10.1021/acsomega.5c00204
ACS Omega 2025, 10, 12530−12542

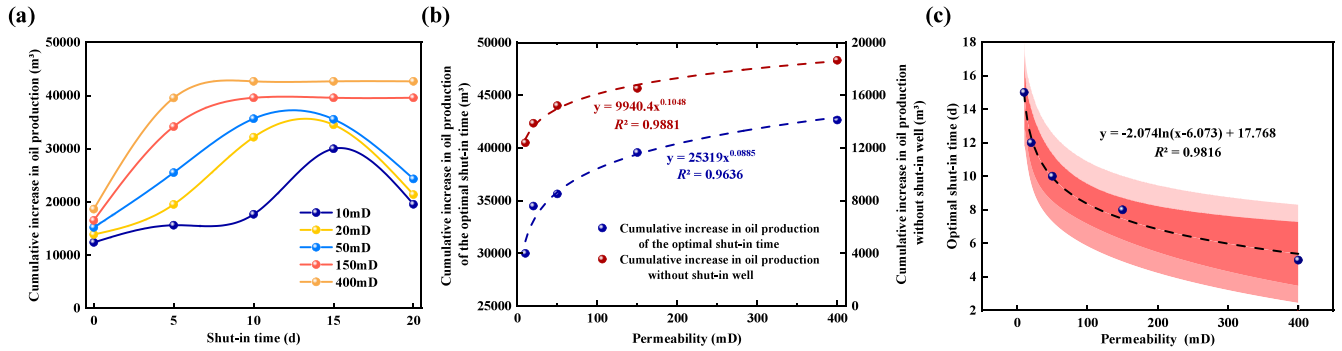

Figure 7. Cumulative increase in oil production by HFAOD (a, b) and optimal shut-in time (c) at different permeabilities

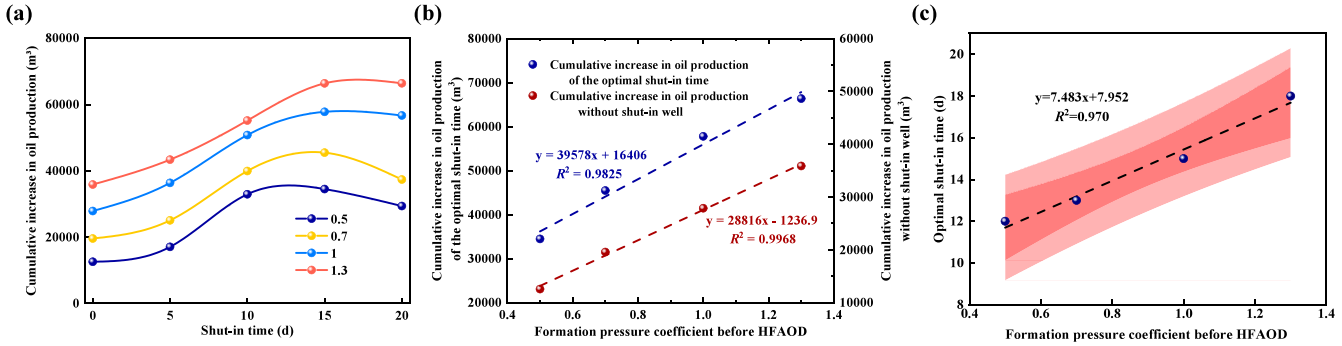

Figure 8. Cumulative increase in oil production by HFAOD (a, b) and optimal shut-in time (c) at different formation pressure coefficients before HFAOD.

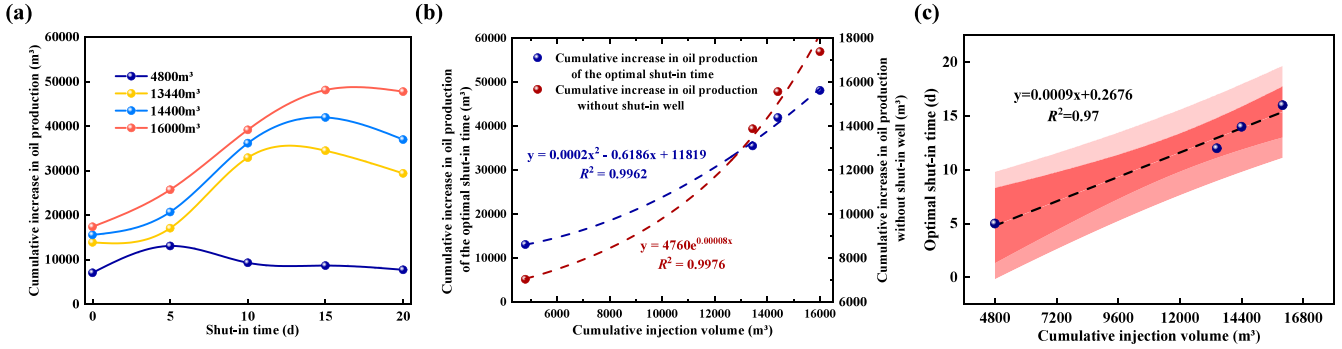

Figure 9. Cumulative increase in oil production by HFAOD (a, b) and optimal shut-in time (c) at different cumulative injection volumes.

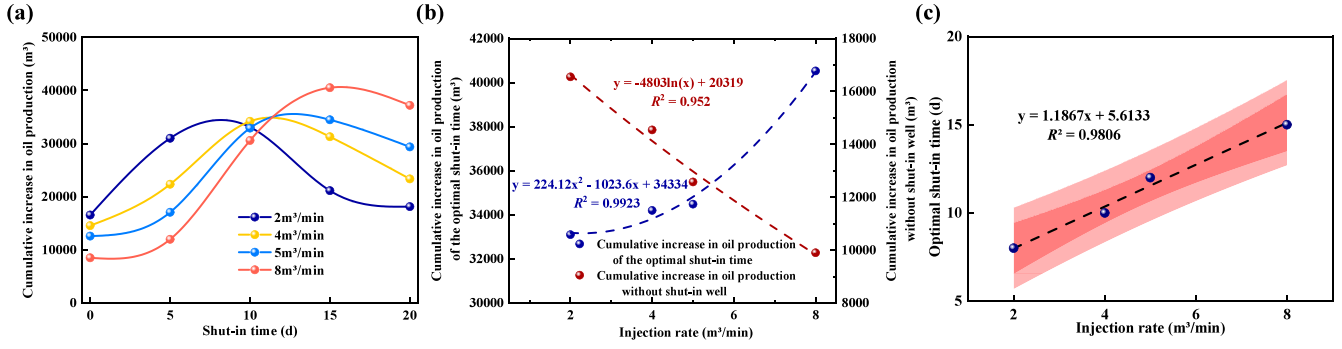

Figure 10. Cumulative increase in oil production by HFAOD (a, b) and optimal shut-in time (c) at different injection rates.

cumulative injection volume, the more the cumulative increase in oil production. This is mainly because a more cumulative injection volume leads to a stronger the effect of formation energy supplementation, allowing for a larger swept volume. The optimal shut-in time of HFAOD gradually increases as the cumulative injection volume increases.

4.1.4. Injection Rate. Considering injection rates of 2, 4, 5, and 8 m^3/min, with corresponding fracture half-lengths of 55,

https://doi.org/10.1021/acsomega.5c00204
ACS Omega 2025, 10, 12530−12542

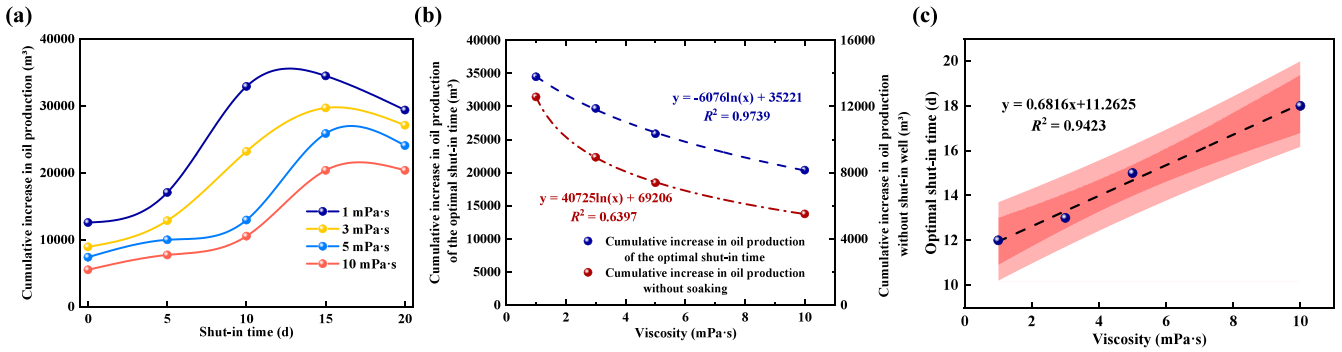

Figure 11. Cumulative increase in oil production by HFAOD (a, b) and optimal shut-in time (c) at different viscosities

118, 153, and 244 m. Figure 10 shows the cumulative increase in oil production and the optimal shut-in time at different injection rates. At the same cumulative injection volume, a higher injection rate leads to greater energy accumulation around the fracture zone at the end of injection, causing the fluid pressure front to advance more quickly during the shut-in well process. But the higher the injection rate, the longer it takes for the fluid pressure to balance. At the optimal shut-in time, a higher injection rate results in a more the cumulative increase in oil production. This is mainly because the higher the injection rate, the longer the fracture half-length, the more geological reserves controlled, the larger the area of the imbibition effect and the more crude oil exchanged back into the fracture. Under the influence of different injection rates, the cumulative increase in oil production by HFAOD is primarily controlled by the fracture half-length at the optimal shut-in time. If the well is not shut in at the end of injection, the cumulative increase in oil production decreases as the injection rate increases. At the same cumulative injection volume, a higher injection rate results in a shorter time for fluid flow in the reservoir, leading to a smaller the swept volume of fluid pressure. The optimal shut-in time of HFAOD gradually increases as the injection rate increases.

4.1.5. Viscosity of HFAOD Fluid. Considering viscosities of 1, 3, 5, and 10 mPa·s, with corresponding fracture half-lengths of 153, 208, 244, and 300 m. Figure 11 shows the cumulative increase in oil production and the optimal shut-in time at different viscosities of HFAOD fluid. As the viscosity of the HFAOD fluid increases, the fracture half-length becomes longer, which is favorable for the cumulative increase in oil production, however, the swept volume of fluid pressure decreases, which is not favorable for the cumulative increase in oil production. Conversely, as the viscosity of the HFAOD fluid decreases, the fracture half-length becomes shorter, which is not favorable for the cumulative increase in oil production, however, the swept volume of fluid pressure increases, which is favorable for the cumulative increase in oil production. The optimal shut-in time of HFAOD gradually increases as the viscosity of the HFAOD fluid increases.

4.2. Analysis of the Main Controlling Factors. Based on the results of the sensitivity analysis, the main controlling factors are determined by using the gray relational analysis method in conjunction with the entropy weight method.[44−47] The optimal shut-in times are used as a reference sequence, different influencing factors are used as a comparative sequence, and a mathematical model of the gray relational method is established. By conjunction with the entropy weight method, the relational degree between the optimal shut-in time and different influencing factors is calculated.

The specific steps are as follows: (1) The optimal shut-in time is defined as the reference sequence, while the cumulative injection volume, formation pressure coefficient before HFAOD, permeability, injection rate, and viscosity of HFAOD fluid are defined as the comparative sequence. (2) The reference and comparison sequences are performed dimensionless, and the absolute differences between them are calculated. (3) The gray relational formula (eq 21) is employed to calculate the relational coefficient between the reference sequence and the comparative sequence. (4) In conjunction with the entropy weight method, the entropy value corresponding to each comparative sequence is calculated using eqs 22-24, ultimately determining the weights of each factor. (5) The relational coefficient and weight are combined using formula 25 to calculate the relational degree of each comparison sequence, thereby determining the main controlling factors affecting the optimal shut-in time.

$$\xi_i(j) = \frac{\Delta(\min) + \rho\Delta(\max)}{\Delta_i(j) + \rho\Delta(\max)} \tag{21}$$

where $\Delta_i(j)$ is the absolute difference, dimensionless; $\xi_i(j)$ is the relational coefficient, dimensionless; ρ is the identification coefficient, dimensionless, $\rho = 0.1$; $\Delta(\min)$ and $\Delta(\max)$ are the minimum and maximum values of the absolute differences, respectively, dimensionless

$$p_{ij} = \frac{y_{ij}}{\sum_{j=1}^{n} y_{ij}} \tag{22}$$

where p_{ij} is the proportion of the j-th influencing factor under the i-th indicator relative to that indicator, dimensionless; y_{ij} is the nondimensionalized data, dimensionless.

$$E_i = k \sum_{j=1}^{n} p_{ij} \ln p_{ij} \tag{23}$$

where E_i is the entropy value of the i-th indicator, dimensionless, $k = -1/\ln n$.

$$\omega_i = \frac{1 - E_i}{m - \sum_{i=1}^{m} E_i} \tag{24}$$

where ω_I is the entropy weight of the i-th indicator, dimensionless.

$$\tau_i = \sum_{j=1}^{n} \omega_i \xi_i(j) (i = 1, 2, \ldots, m) \tag{25}$$

https://doi.org/10.1021/acsomega.5c00204
ACS Omega 2025, 10, 12530−12542

where τ_i is the relational degree of the i-th comparative sequence, dimensionless.

Finally, the weights of different influencing factors are determined (Table 4). The influence degree of different factors

Table 4. Analysis Results of the Main Controlling Factors for the Optimal Shut-In Time of HFAOD

Number	Parameter	Weight
1	Cumulative injection volume	0.2919
2	Formation pressure coefficient before HFAOD	0.2611
3	Permeability	0.231
4	Injection rate	0.1431
5	Viscosity of HFAOD fluid	0.0739

on the optimal shut-in time of HFAOD is as follows: cumulative injection volume > formation pressure coefficient before HFAOD > permeability > injection rate > viscosity of the HFAOD fluid. The main controlling factors that affect the optimal shut-in time of HFAOD are the cumulative injection volume, formation pressure coefficient before HFAOD, and permeability. These factors should be given special attention when optimizing the shut-in time of HFAOD.

5. CONCLUSIONS

(1) A coupled model of HFAOD encompassing injection, shut-in well, and production is established and shows good agreement with production data obtained on site. The calculation accuracies for cumulative oil production, cumulative water production and the bottom hole pressure are 99.19%,99.84% and 86.43% for well $L^{\#}$, and 98.46%, 85.1% and 85.88% for well $W^{\#}$.

(2) The primary function of the shut-in well is to enhance the effect of formation energy supplementation after injection, thereby further increasing the swept volume, controlling greater geological reserves, and ultimately enhancing oil recovery. In the early stage of shut-in well, displacement plays a dominant role. A larger geological reserve is controlled by fluid pressure diffusion. In the later stage of shut-in well, imbibition plays a dominant role. The crude oil far from the fracture zone is exchanged back into the fracture zone.

(3) The higher the permeability, the lower the formation pressure coefficient before HFAOD, the slower the injection rate, the lower the viscosity of the HFAOD fluid, the less the cumulative injection volume, and the shorter the optimal shut-in time. The main controlling factors that affect the optimal shut-in time of HFAOD are the cumulative injection volume, formation pressure coefficient before HFAOD, and permeability. These factors should be given special attention when optimizing the shut-in time of HFAOD.

AUTHOR INFORMATION

Corresponding Author

Mingxuan Chu − *Laboratory of Enhanced Oil Recovery of Education Ministry, Northeast Petroleum University, Daqing 163318, P. R. China;* orcid.org/0009-0004-8604-1627; Email: cmx_3526@163.com

Authors

Baojiang Duan − *CNOOC Energy Tech-Drilling & Production Co., Tianjin 300450, P. R. China*

Qi Li − *CNOOC Energy Tech-Drilling & Production Co., Tianjin 300450, P. R. China*

Zhenhua Cai − *CNOOC Energy Tech-Drilling & Production Co., Tianjin 300450, P. R. China*

Kang Jiang − *CNOOC Energy Tech-Drilling & Production Co., Tianjin 300450, P. R. China*

Fengjiao Wang − *Laboratory of Enhanced Oil Recovery of Education Ministry, Northeast Petroleum University, Daqing 163318, P. R. China;* orcid.org/0000-0001-8414-3049

Yikun Liu − *Laboratory of Enhanced Oil Recovery of Education Ministry, Northeast Petroleum University, Daqing 163318, P. R. China*

Mengyao Ren − *Laboratory of Enhanced Oil Recovery of Education Ministry, Northeast Petroleum University, Daqing 163318, P. R. China*

Zhiming Yan − *Laboratory of Enhanced Oil Recovery of Education Ministry, Northeast Petroleum University, Daqing 163318, P. R. China*

Qiang Xie − *No. 10 Oil Production Plant, Daqing Oilfield Co., Ltd., Daqing City, Heilongjiang Province 163315, P. R. China*

Complete contact information is available at: https://pubs.acs.org/10.1021/acsomega.5c00204

Notes

The authors declare no competing financial interest.

ACKNOWLEDGMENTS

This work was the Major Special Project for Energy Development of CNOOC (HFKJ-ZX-GJ-2023-02).

NOMENCLATURE

K_f	the absolute permeability of the fracture, mD
K_m	the absolute permeability of the matrix, mD
K_{ro}	the respectively the relative permeability of the oil phase, dimensionless
K_{rw}	the respectively the relative permeability of the water phase, dimensionless
D	the depth of reservoir, m
S_{fo}	the saturation of oil phase in the fracture, dimensionless
S_{fw}	the saturation of water phase in the fracture, dimensionless
S_{mo}	the saturation of the oil phase in the matrix, dimensionless
S_{mw}	the saturation of the water phase in the matrix, dimensionless
B_0	the volume factor of the oil phase, dimensionless
B_w	the volume factor of the water phase, dimensionless
μ_o	the viscosity of the oil phase, mPa·s
μ_w	the viscosity of the water phase, mPa·s
p_0	the initial pore pressure, MPa
p_{fo}	the pressure of the oil phase in the fracture, MPa
p_{mo}	the pressure of the oil phase in the matrix, MPa
p_{fw}	the pressure of the water phase in the fracture, MPa
p_{mw}	the pressure of the water phase in the matrix, MPa
ρ_o	the density of oil phase, kg/m^3
ρ_w	the density of water phase, kg/m^3
ρ_R	the rock density, kg/m^3
α_o	the shape factor of the oil phase, dimensionless
α_w	the shape factor of the water phase, dimensionless
α_{ws}	the shape factor of HFAOD fluid phase, dimensionless
ϕ_f	the porosity of the fracture, dimensionless

https://doi.org/10.1021/acsomega.5c00204
ACS Omega 2025, 10, 12530−12542

$\phi_{0,f}$ the initial porosity of the fracture, dimensionless
ϕ_m the porosity of the matrix, dimensionless
$\phi_{0,m}$ the initial porosity of the matrix, dimensionless
m^a_s the adsorption mass of HFAOD fluid, kg/m^3
m^D_s the diffusive mass flux of HFAOD fluid, kg/(m^2·s)
C_f the porosity compression coefficient of the fracture, MPa^{-1}
C_m the porosity compression coefficient of the matrix, MPa^{-1}
C_s the mass concentration of HFAOD fluid, kg/m^3
C^a_s the adsorption concentration of HFAOD fluid, kg/kg
C^D_s the diffusion concentration of HFAOD fluid, kg/kg
D_s the diffusion coefficient of HFAOD fluid, m^2/s
E_f the stress sensitivity coefficient of fracture permeability, MPa^{-1}
E_m the stress sensitivity coefficient of matrix permeability, MPa^{-1}
N_c^{max} the capillary number of maximum concentrations of HFAOD fluid, dimensionless
N_c^{min} the capillary number of minimum concentrations of HFAOD fluid, dimensionless
N_c the capillary number, dimensionless
p_{cres} the capillary force of reservoir condition, MPa
p_{clab} the capillary force of experimental condition, MPa
σ_{res} the interfacial tension of reservoir condition, MPa
σ_{lab} the interfacial tension of experimental condition, MPa
θ_{res} the wetting angle of reservoir condition, °
θ_{lab} the wetting angle of experimental condition, °
S_{wi} the irreducible water saturation, dimensionless
S_{or} the residual oil saturation, dimensionless
$\Delta_i(j)$ the absolute difference, dimensionless
$\xi_i(j)$ the relational coefficient, dimensionless
ρ the identification coefficient, dimensionless
$\Delta(\min)$ the minimum values of the absolute differences, dimensionless
$\Delta(\max)$ the maximum values of the absolute differences, dimensionless
p_{ij} the proportion of the j-th influencing factor under the i-th indicator relative to that indicator, dimensionless
y_{ij} the nondimensionalized data, dimensionless
E_i the entropy value of the i-th indicator, dimensionless
ω_i the entropy weight of the i-th indicator, dimensionless
τ_i the correlation value of the i-th comparison sequence, dimensionless

Abbreviation

HFAOD Hydraulic fracturing assisted oil displacement

REFERENCES

(1) Feng, Q.; Zhou, J. C.; Li, S. S.; Chen, X. C.; Sun, Y. N.; Zhang, X. R.; Gao, P.; Zhang, F.; She, Y. H. Research on characterization technology and field test of biological nano-oil displacement in offshore medium-and low-permeability reservoirs. *ACS Omega* **2022**, *7* (44), 40132−40144.

(2) Liu, Y. K.; Wang, F. J.; Wang, Y. M.; Li, B. H.; Dong, Z.; Zhi, J. Q.; Sun, S.; Wang, X.; Deng, Q. J.; Xu, H. The mechanism of hydraulic fracturing assisted oil displacement to enhance oil recovery in low and medium permeability reservoirs. *Pet. Explor. Dev.* **2022**, *49* (4), 864−873.

(3) Zheng, W.; Tan, X. H.; Jiang, W. D.; Xie, H. J.; Pei, H. H. Investigation of nanoclay-surfactant-stabilized foam for improving oil recovery of steam flooding in offshore heavy oil reservoirs. *ACS Omega* **2021**, *6* (35), 22709−22716.

(4) Yu, Q. N.; Liu, Y. K.; Liang, S.; Tan, S.; Sun, Z.; Yu, Y. Experimental study on surface-active polymer flooding for enhanced oil recovery: A case study of Daqing placanticline oilfield, NE China. *Pet. Explor. Dev.* **2019**, *46* (6), 1206−1217.

(5) Wu, B.; Wu, G.; Wang, L.; Lou, Y.; Liu, S.; Yin, B.; Li, S. Study on fracturing parameters optimization of horizontal wells in low-permeability reservoirs in South China Sea. *Processes* **2023**, *11*, 2999.

(6) Wang, S.; Liang, Y. P.; Feng, Q. H.; Javadpour, F. Sticky layers affect oil transport through the nanopores of realistic shale kerogen. *Fuel* **2022**, *310*, 122480.

(7) Li, Y. W.; Xu, L.; Gou, Y. H.; Du, T.; Xiao, Y. H. A calculation model for hydraulic fracture height considering interlayer slip energy dissipation. *SPE J.* **2025**, SPE-224426-PA.

(8) Wang, Q.; Zhao, J. Z.; Hu, Y. Q.; Ren, L.; Zhao, C. N. Shut-in time optimization after fracturing in shale oil reservoirs. *Pet. Explor. Dev.* **2022**, *49* (3), 671−683.

(9) Wang, F.; Ruan, Y. Q.; Chen, Q. Y.; Zhang, S. C. A pressure drop model of post-fracturing shut-in considering the effect of fracturing-fluid imbibition and oil replacement. *Pet. Explor. Dev.* **2021**, *48* (6), 1440−1449.

(10) Zeng, B.; Dong, E.; Yao, Z.; Song, Y.; Xiong, Z.; Huang, Y.; Gou, X.; Hu, X. Strategies for optimizing shut-in time: New insights from shale long-term hydration experiments. *Processes* **2024**, *12* (6), 1096−1096.

(11) Liu, Y. F.; Zhu, Y. W.; Liao, H. Y.; Yu, H. M.; Fang, X.; Zhang, Y. Mathematical model of imbibition replacement and optimization of soaking time for massively fractured tight oil reservoirs. *ACS omega* **2023**, *8* (38), 35107−35120.

(12) Wei, J. G.; Shang, D. M.; Zhao, X. Q.; Zhou, X. F.; Yang, Y.; Du, M. Experimental study on production characteristics and enhanced oil recovery during imbibition and huff-n-puff injection in shale reservoir. *Capillarity* **2024**, *12* (2), 41−56.

(13) Bui, B. T.; Tutuncu, A. N. Contribution of osmotic transport on oil recovery from rock matrix in unconventional reservoirs. *J. Pet. Sci. Eng.* **2017**, *157*, 392−408.

(14) Wei, Q.; Li, Z. P.; Wang, X. Z.; Bai, R. T.; Wang, C.; Li, H. Mechanism and influence factors of imbibition in fractured tight sandstone reservoir: An example from Chang 8 reservoir of Wuqi area in Ordos Basin. *Pet. Geol. Recovery Effic.* **2016**, *23*, 102−107.

(15) Wang, Y. J.; Liu, H. Q.; Li, Y.; Wang, Q. Numerical simulation of spontaneous imbibition under different boundary conditions in tight reservoirs. *ACS omega* **2021**, *6* (33), 21294−21303.

(16) Wang, F. J.; Xu, H.; Liu, Y. K.; Du, Q. L.; Zhang, D. The mechanism of hydraulic fracturing-assisted oil displacement technique applied to enhance oil recovery by high-pressure reduced adsorption. *Acta Petrol. Sin.* **2024**, *45*, 403−411.

(17) Xu, J. G.; Liu, R. J.; Liu, H. X. Optimization of shut-in time based on saturation rebalancing in volume-fractured tight oil reservoirs. *Pet. Explor. Dev.* **2023**, *50* (06), 1445−1454.

(18) Zhu, W.; Liu, Y.; Li, Z.; Yue, M.; Kong, D. Study on pressure propagation in tight oil reservoirs with stimulated reservoir volume development. *ACS Omega* **2021**, *6* (4), 2589−2600.

(19) Abdelaziz, A.; Ha, J.; Li, M.; Magsipoc, E.; Sun, L.; Grasselli, G. Understanding hydraulic fracture mechanisms: From the laboratory to numerical modelling. *Adv. Geo-Energy Res.* **2023**, *7* (1), 66−68.

(20) Wang, F. J.; Xu, H.; Liu, Y. K.; Meng, X. H.; Liu, L. C. F. Mechanism of low chemical agent adsorption by high pressure for hydraulic fracturing-assisted oil displacement technology: A study of molecular dynamics combined with laboratory experiments. *Langmuir* **2023**, *39* (46), 16628−16636.

(21) Yan, Z. M.; Wang, F. J.; Liu, Y. K.; Zhang, J.; Liu, L.; Gao, M. Y. Effects of CO_2 pressure on the dynamic wettability of the kerogen surface: Insights from a molecular perspective. *Appl. Surf. Sci.* **2025**, *694*, 162822.

(22) Wang, J.; Liu, H. Q.; Qian, G. B.; Yong, C. P. Mechanisms and capacity of high-pressure soaking after hydraulic fracturing in tight/shale oil reservoirs. *Pet. Sci.* **2021**, *18* (2), 546−564.

(23) Yang, L.; Wang, H. K.; Zou, Z. Y.; Jiang, Q. P.; Zhang, J. K.; Xu, J. C.; Cai, J. C. Effects of fracture characteristics on spontaneous imbibition in a tight reservoir. *Energy Fuels* **2021**, *35* (19), 15995−16006.

https://doi.org/10.1021/acsomega.5c00204
ACS Omega 2025, 10, 12530−12542

(24) Wang, J.; Liu, H. Q.; Xia, J.; Liu, Y. T.; Hong, C.; Meng, Q. B.; Gao, Y. Numerical simulation of imbibition and oil recovery mechanism in fractured reservoirs. *Pet. Explor. Dev.* **2017**, *44*, 761−770.
(25) Zhang, T. T.; Li, Z. P.; Gao, M. W.; Wang, L.; Adenutsi, C. D.; You, Q. Experimental and numerical simulation research on counter-current imbibition distance in tight oil reservoirs. *J. Mol. Liq.* **2023**, *389*, 122791.
(26) Wang, F.; Chen, Q. Y.; Zhang, J. C.; Ruan, Y. Q.; Zhuang, Y.; Zhu, J.; Zhang, S. C. Numerical investigation of oil-water exchange behaviors in shale during post-fracturing soaking periods. *Front. Earth Sci.* **2021**, *9*, 735972.
(27) Cai, J. C.; Qin, X. J.; Wang, H.; Xia, Y. X.; Zou, S. M. Pore-scale investigation of forced imbibition in porous rocks through interface curvature and pore topology analysis. *J. Rock Mech. Geotech. Eng.* **2025**, *17* (1), 245−257.
(28) Xu, R. L.; Guo, T. K.; Xue, X. J.; Chen, W. B.; Qu, Z. Q.; Chen, M.; Hu, Z. P. Numerical simulation of fracturing and imbibition in shale oil horizontal wells. *Pet. Sci.* **2023**, *20*, 2981−3001.
(29) Du, S. H.; Bai, L. Future potential research hotspots on the precise integration of geology and engineering in low-permeability oil reservoirs. *Adv. Geo-Energy Res.* **2024**, *14* (1), 4−7.
(30) Chen, X.; Liao, K.; Lv, Z.; Zhu, J.; Wang, J. C.; Li, Y. Q.; Wang, F. Numerical simulation study on optimal shut-in time in Jimsar shale oil reservoir. *Front. Energy Res.* **2022**, *10*, 849064.
(31) Liang, Y. P.; Wang, S.; Feng, Q. H.; Zhang, M. Q.; Cao, X. P.; Wang, X. K. Ultrahigh-resolution reconstruction of shale digital rocks from FIB-SEM images using deep learning. *SPE J.* **2024**, *29* (03), 1434−1450.
(32) Gu, T.; Yan, L.; Fan, T.; Guo, X. C.; Fan, F.; Zhang, Y. J. Numerical simulation study of pressure transfer based on the integration of fracturing, Shut-in and production in tight reservoirs. *Sustainability* **2023**, *15* (16), 12184.
(33) Tangparitkul, S.; Sukee, A.; Jiang, J.; Tapanya, C.; Fongkham, N.; Yang, H. Role of interfacial tension on wettability-controlled fluid displacement in porous rock: A capillary-dominated flow and how to control it. *Capillarity* **2023**, *9* (3), 55−64.
(34) Zhang, Q. T.; Liu, W. C.; Wei, J. X.; Taleghani, A. D.; Sun, H.; Wang, D. B. Numerical simulation study on temporary well shut-in methods in the development of shale oil reservoirs. *Energies* **2022**, *15* (23), 9161.
(35) Cao, G. S.; Cheng, Q. C.; Liu, Y.; Bu, R. X.; Zhang, N.; Wang, P. L. Influencing factors of surfactant stripping crude oil and spontaneous imbibition mechanism of surfactants in a tight reservoir. *ACS omega* **2022**, *7* (22), 19010−19020.
(36) Yan, Z. M.; Wang, F. J.; Liu, Y. K.; Wang, P. A coupled matrix-fracture productivity calculation model considering low-velocity non-Darcy flow in shale reservoirs. *Fuel* **2024**, *357*, 129845.
(37) Wang, S.; Zhang, M. Q.; Zhang, Y. L.; Lei, Z. D.; Feng, Q. H.; Xu, S. Q.; Zhang, J. Y. Mechanisms of CO_2 huff and puff enhanced oil recovery and storage within shale nanopores. *Chem. Eng. J.* **2025**, *506*, 160098.
(38) Zhang, X. C.; Yang, Y. J.; Liu, J. L.; Gao, Z. X.; Huang, X. Q.; Zeng, F. H. Numerical simulation of reasonable soaking time in development of shale oil. *J. Xi'an Shiyou Univ., Nat. Sci. Ed.* **2021**, *36* (03), 71−76.
(39) Yan, Z. M.; Wang, F. J.; Liu, Y. K.; Fan, J. L.; Wang, P.; Chu, M. X. Dynamic wetting of a CO_2-H_2O-montmorillonite system using molecular dynamics. *Fuel* **2024**, *377*, 132787.
(40) Li, Y. W.; Peng, G. B.; Tang, J. Z.; Zhang, J.; Zhao, W. C.; Liu, B.; Pan, Y. S. Thermo-hydro-mechanical coupling simulation for fracture propagation in CO_2 fracturing based on phase-field model. *Energy* **2023**, *284*, 128629.
(41) Wang, F.; Chen, Q. Y.; Ruan, Y. Q. Hydrodynamic equilibrium simulation and shut-in time optimization for hydraulically fractured shale gas wells. *Energies* **2020**, *13* (4), 961.
(42) Ge, Y. L.; Li, S. R. Numerical computation method for solving flow model of ASP flooding based on full implicit finite difference. *Adv. Appl. Math.* **2018**, *7* (4), 476−493.
(43) Wei, F.; Tang, M. G.; Deng, X.; Zhang, Y. L.; Wang, F. J.; Liu, Y. K.; Yan, G. L.; Wu, Q. Coupling study of fracture propagation-filtration-seepage during hydraulic fracturing assisted oil displacement in offshore low-permeability reservoirs. *ACS omega* **2025**, *10* (1), 1761−1771.
(44) Zhang, J. C.; He, X. R.; Zhou, W. S.; Geng, Z. L.; Tang, E. G. Main controlling factors of interlayer interference in big intervals commingled production oil wells. *J. Southwest Pet. Univ., Sci. Technol. Ed.* **2015**, *37*, 101−106.
(45) Hu, J. H.; Zhao, H. P.; Du, X. F.; Zhang, Y. An analytical model for shut-in time optimization after hydraulic fracturing in shale oil reservoirs with imbibition experiments. *J. Pet. Sci. Eng.* **2022**, *210*, 110055.
(46) Li, Y. W.; Peng, G. B.; Du, T.; Jiang, L. L.; Kong, X. Z. Advancing fractured geothermal system modeling with artificial neural network and bidirectional gated recurrent unit. *Appl. Energy* **2024**, *372*, 123826.
(47) Jia, P.; Ke, X. Z.; Li, Y.; Peng, C.; Cheng, L. S. Dynamic response characteristics of oil and water distribution during the shut-in period after hydraulic fracturing in shale oil reservoirs. *Front. Earth Sci.* **2022**, *10*, 996087.

https://doi.org/10.1021/acsomega.5c00204
ACS Omega 2025, 10, 12530−12542